I S A V

Journal of Theoretical and Applied Vibration and Acoustics

journal homepage: http://tava.isav.ir

Design and simulation of acoustic metamaterial luneburg lenses for predetermined focal points

Mohammad Naeim Moradi [a], **Maryam Ghassabzadeh Saryazdi** [b,*], **Abdolreza Ohadi** [c]

[a] *PhD student, Acoustics Research Laboratory, Mechanical Engineering Department, Amirkabir University of Technology (Tehran Polytechnic), Tehran, IRAN.*

[b] *Assistant Professor, Vehicle Technology Research Institute, Amirkabir University of Technology (Tehran Polytechnic), Tehran, IRAN.*

[c] *Professor, Acoustics Research Laboratory, Mechanical Engineering Department, Amirkabir University of Technology (Tehran Polytechnic), Tehran, IRAN.*

Research Article

ARTICLE INFO

Article history:
Received 26 May 2025

Received in revised form
16 August 2025

Accepted 30 August 2025

Available online 11 June 2026

Keywords:
Acoustic metamaterials

Luneburg lens

Predetermined focal points

Elastic waves

ABSTRACT

This paper presents the design and simulation of acoustic metamaterial lenses that focus elastic waves at predetermined focal points. The modified Luneburg refractive index profile is used in the design process to define focal point locations, a capability not previously explored in elastic wave research. This new approach is important because it enables more precise spatial control of waves, resulting in enhanced resolution for elastic wave focusing applications. Three lenses, each targeting specific focal points, are designed by proposing hexagonal unit cells containing blind holes with varying diameters. Dispersion curves are calculated by finite element simulations to determine wave properties of unit cells, including refractive indices. These unit cells provide a wide range of refractive indices (1.0314-1.4959) at the design frequency of 50 kHz, which is suitable for constructing Luneburg lenses. Unit cells are then arranged according to the discretized refractive index profiles to form the lenses. Numerical simulations validate effective wave focusing at the intended focal points (F=R, 1.5R, 2R) with three lenses. The highest amplification of waves and the narrowest focal zone are for the lens with F=R. As the focal point shifts toward 2R, wave distribution becomes scattered along the focal axis. Decay length

* Corresponding author.
E-mail address: mghsaryazdi@aut.ac.ir (M. Ghassabzadeh Saryazdi)

http://dx.doi.org/10.22064/tava.2025.2061787.1265

analysis of F=1.5R and 2R lenses indicates their suitability for long distribution of high-velocity regions. Frequency-dependent simulations across 46–52 kHz reveal that all lenses maintain efficient focusing between 49–51 kHz. At more distant off-design frequencies, amplifications result from refractive index shifts that misalign the focal point.

1. Introduction

In recent years, there has been growing interest in acoustic metamaterials (AMs). AMs are artificial materials that can control sound waves through innovative mechanisms such as local resonances or geometrical arrangements, often achieving unnatural effects such as negative refraction. Acoustic metamaterials have potential applications in various industrial and medical fields [1-5] as acoustic absorbers [6], barriers [7], lenses [8-10] and cloaks [11]. Acoustic lenses are devices that are specifically designed to focus sound waves at one or more focal points. The unique properties of lenses are useful for elastic wave applications like sensing and damage detection in solids [12] , non-destructive testing [13] , and energy harvesting [14]. The current study demonstrates the potential of these lenses in precisely controlling acoustic/elastic wave propagation.

The literature on acoustic metamaterial lenses highlights various methods for wave control, which lead to wave focusing. In a related study in 2022, Zhao et al. [15] explored the Rays Inserting Method (RIM), to design acoustic lenses for flexural wave manipulation by varying the thickness of thin plates to achieve a desired refractive index profile. Additionally, Yang et al. [16] designed a negative refraction index lens by proposing a structure of rotating scatterers on a plate containing periodic perforated three-fan holes. Scatterers with different rotation angles exhibit variations in the dispersion curve, which is related to a specific negative refraction index. Their designed lens had a fixed focal point in the frequency range of 16 to 19kHz and was analyzed for energy harvesting. In a paper in 2024, Quadrelli et al. [17] reported the development of a metamaterial with both negative dynamic mass and stiffness, which was capable of negative refraction of elastic flexural waves, eventually resulting in a focusing lens. The double-negative behavior was obtained by both mechanical resonators and piezoelectric patches with inductive resonant shunts. Zhao et al. [18] introduced a structural Luneburg lens for broadband ultralong subwavelength focusing, utilizing two concentric circular regions with varying thickness in a thin plate to achieve double foci and control energy flow between the two focal spots. Their results showed the achievement of a large full-length at half maximum (*FLHM*) up to 15λ at the focusing region, while the full width at half maximum (*FWHM*) is limited to a subwavelength scale. It is worth mentioning that their primary focus was on achieving a long focal region rather than precise control over the exact locations of the focal points, the latter being the main target of the present study. Tol et al. [19] designed a gradient index lens for elastic wave energy harvesting, using an array of blind holes with varying diameters in an aluminum plate, though their lens lacked omnidirectionality and used square unit cells. Building on this, Tol et al. [20] developed a phononic crystal Luneburg lens with omnidirectional elastic wave focusing, though without control over the focal point.

This study presents a lens design method based on a structure comprising hexagonal unit cells with blind holes, which offers greater structural integrity than previous fully perforated and variable thickness structures. Adjusting the diameter of the blind holes in this type of unit cell provides the desired acoustic properties of refractive index for the lens design. This offers a wide range of refractive indices at the design frequency of 50 *kHz*. The proposed design method in this paper enables the achievement of arbitrarily positioned focal points of elastic waves, which is crucial for precise elastic wave control in real-world applications of the lens. This is achieved using different variants of the proposed structure to approximate the modified Luneburg refractive index profile. For this reason, three distinct lenses are designed. Their performance is validated through finite element simulations in COMSOL. In addition to evaluating the performance of the lenses at the design frequency, a frequency-dependent study is conducted to examine how frequency affects wave concentration behavior. The remainder of this paper is organized as follows. Section 2 comprehensively explains the procedure for lens design. Section 3 covers the finite element simulations, presenting the results and analyzing them in detail. Lastly, Section 4 concludes the paper by summarizing the key findings of the study.

2. Design and simulation principles

Among acoustic lenses, gradient refractive index lenses (GRIN) have a spatially variable refractive index within the metamaterial, thereby enabling easy manipulation of incident waves. Luneburg lens (originally in optics) is a symmetric gradient-index lens that can focus acoustic waves from any direction to an arbitrary point and thus is chosen as a suitable lens for this study [21]. The governing equation of the modified acoustic Luneburg lens [10] presents the refractive index *n(r)* at any point within the Luneburg lens as a function of the radial distance *r* from the center of the lens [10]:

$$n(r) = \frac{\sqrt{F^2 + R^2 - r^2}}{F} \tag{1}$$

where *R* is the radius of the lens, and *F* is the location of the focal point. The traditional profile of the Luneburg lens can be achieved by using *F=R* in Eq. (1). Based on this governing equation, which is plotted in Figure 1. (a), for three cases of *F = R*, 1.5*R*, 2*R*, the refractive index is highest at the center of the lens and decreases radially towards the edge. A low refractive index at the outer boundaries results in impedance matching with the background medium. Furthermore, the smooth transition of refractive index allows sound waves to travel along curved paths within the lens. Therefore, acoustic waves can enter and travel within the lens without any reflection. Figure 1. (b) is obtained by ray trajectory simulations using COMSOL's geometrical optics interface. A collimated array of rays is released into the sphere in which its only needed material property is defined with the modified Luneburg refractive index profile of Eq. (1). This figure shows how waves behave in each of the three mentioned focal distance cases. It can be seen that changing the refractive index profile from *F=R* to *F=1.5R* or *F=2R* results in an extended focal region rather than a sharp focal point. This indicates that the modified Luneburg lens inherently produces a broader convergence zone as the target focal distance increases. Theoretically, this behavior is the direct result of flattening the refractive index profile as the focal point is moved farther from the lens surface, as indicated in Figure 1. (a). A smaller variation in refractive index across the lens

causes less bending of the incident waves, leading to a longer convergence path. However, an extended focal region is accepted in the current study to reach the goal of acoustic metamaterial lenses for elastic waves with predetermined focal points. Further investigations similar to those presented by Zhao et al. [10] for acoustic waves are required in future studies in this context to optimize the lens and reduce this aberration.

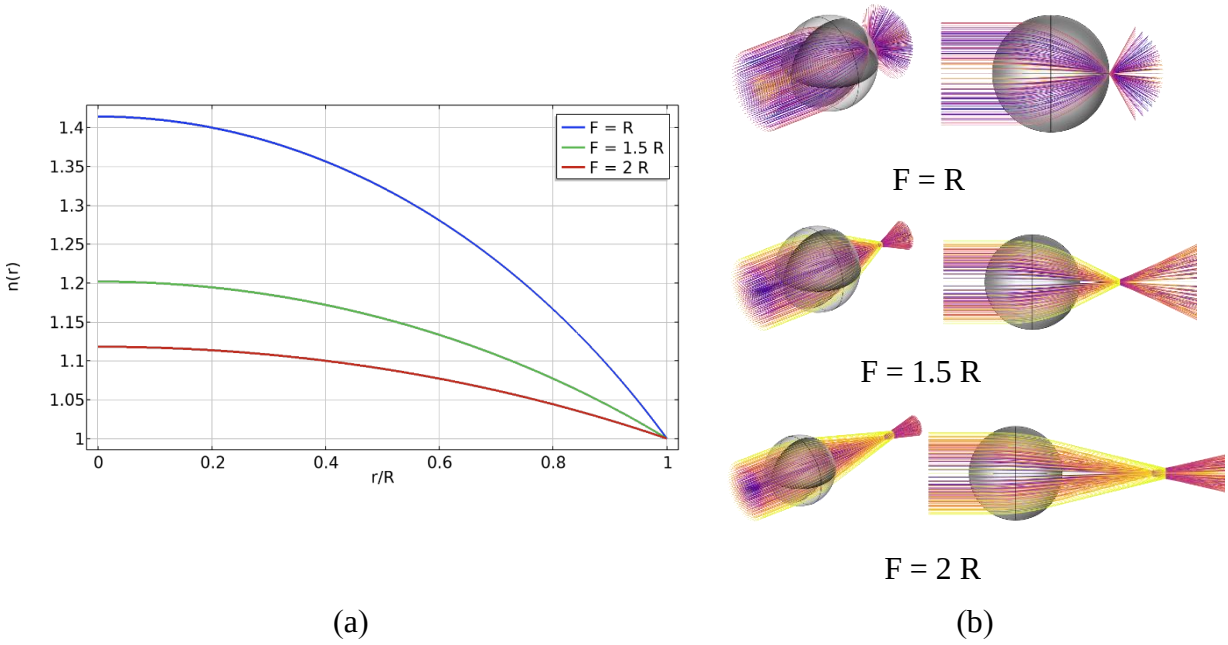

Fig. 1. a) Refractive index profile of modified Luneburg lenses. b) Ray trajectories of the Luneburg lens with various focal points.

To create a practical Luneburg lens, a unit cell that can produce a spatially varying refractive index should be proposed. For this reason, many concepts have been introduced through variations in material or size. Examples include periodically arranged cross-shaped cells [10], variable thickness plates [15], and perforated plates with different hole sizes [16]. As demonstrated by Figure 2. (a), hexagonal unit cells with blind holes of various diameters in the middle are proposed in this study. This choice results in a hexagonal final shape of the lens, which is a close shape to a circular Luneburg lens, as shown in Figure 2. (b). The use of a blind-hole design, rather than a basic perforated plate, enhances the structural integrity of the lens.

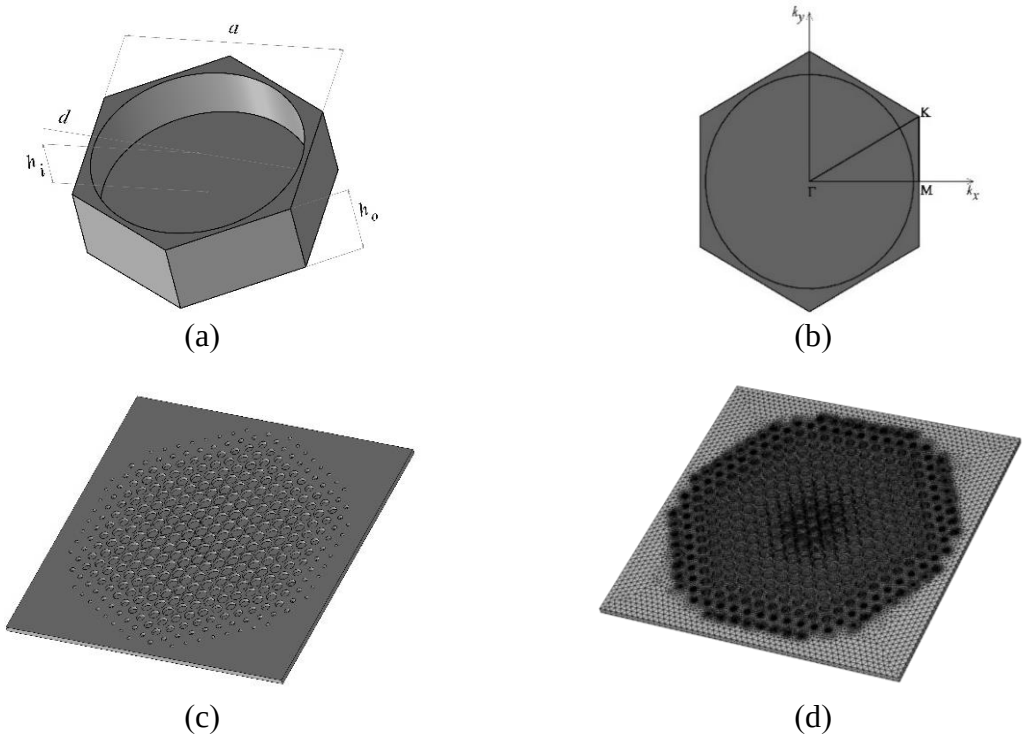

Fig. 2. a) Hexagonal unit cell. b) Irreducible Brillouin zone. c) Luneburg lens designed based on the refractive index profile with F=R. d) Meshed geometry of the lens.

The refractive indices of unit cells should be calculated to properly arrange the cells next to each other and form the complete lens. This is done by deriving dispersion curves, which provide insight into how waves propagate through the periodic structure at different frequencies. Calculating dispersion curves involves solving the eigenvalue problem derived from the Floquet-Bloch theorem applied to the wave equation in solids. The wave equation for elastic wave propagation in a solid is given by [22]:

$$\nabla.(C:\nabla u) = \rho \frac{\partial^2 u}{\partial t^2} \tag{2}$$

where C is the stiffness tensor, u is the displacement vector, and ρ is the density of the material. According to the Floquet-Bloch theorem, the solution to the wave equation in a periodic structure can be expressed as [23]:

$$u(r) = u_p(r) e^{ik.r} \tag{3}$$

where $u_p(r)$ is a periodic function with the same periodicity as the crystal structure and satisfies $u_p(r+a) = u_p(r)$ with a as the lattice constant, and $e^{ik.r}$ is a phase factor with k representing the wavevector. Substituting this form into the wave equation with periodic coefficients yields an

eigenvalue problem, which is solved to obtain the dispersion relation $\omega=\omega(k)$. The computation of the dispersion relation is performed within the first Brillouin zone, which is the fundamental region in reciprocal (k_x-k_y) space for periodic structures. Due to the symmetry of the crystal, it is sufficient to compute the dispersion relation within the irreducible part of the Brillouin zone rather than over the entire lattice, significantly reducing computational effort. This zone captures the structure's unique wave propagation, enabling the prediction of wave behavior throughout the entire periodic medium.

The dispersion curves are calculated (shown and verified with reference in Figure 3) using finite element method (FEM) simulations in COMSOL Multiphysics. The eigenvalue problem is solved numerically over the irreducible Brillouin zone (IBZ). The IBZ is shown in Figure 2. (b). By parametric sweeping the wave number of k_x along GM from 0 to π/a, eigenfrequencies are computed at each wave number value. This eigenfrequency analysis is performed for each unit cell under Floquet periodic boundary conditions, where a phase shift corresponding to the wave vector of k_x is imposed between opposite sides of the unit cell. For each wave number of k_x, this process yields the natural frequencies that the unit cell can resonate with. In other words, the dispersion curve contains the allowable frequency-wave vector combinations inside the unit cell. Changing the blind hole diameters alters these combinations; therefore, each unit cell with a given set of blind hole diameters has a specific dispersion curve.

The hexagonal unit cell is considered to have constant dimensions of short diagonal distance a = 8 *mm*, plate thickness (outer side) h_o = 3.175 *mm*, and hole depth (inner side) h_i = 2.175 *mm*. However, the diameter of the blind hole (d) is treated as a design variable and adjusted to achieve a desired refractive index.

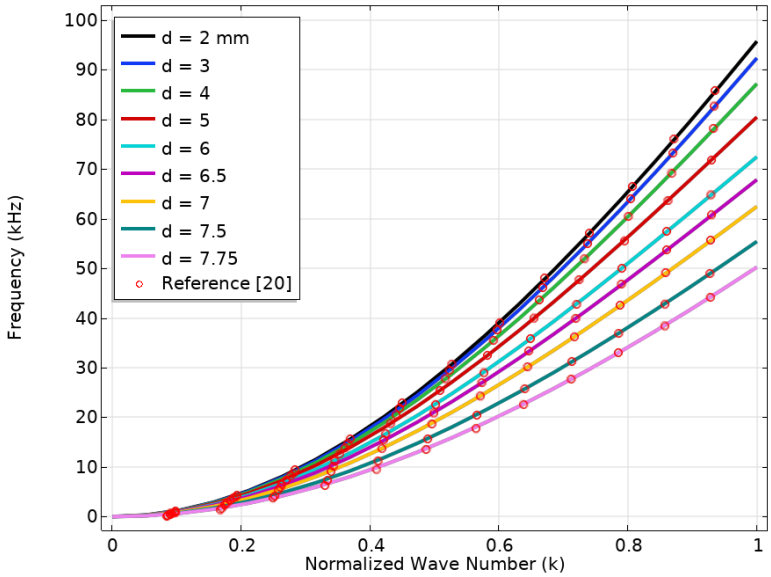

Fig. 1. Dispersion diagram of unit cells of different diameter blind holes.

By examining the relationship between the wave vector and frequency (the dispersion relation), the material's dispersion properties, such as wave propagation speed, can be determined. The refractive index can then be calculated using Eq. (4) as follows [20]:

$$n = \frac{c}{c_{\Gamma M}} \tag{4}$$

in which $c_{\Gamma M}$ is the phase velocity in the ΓM direction of the unit cell and c is the reference phase velocity of the first antisymmetric wave mode in a homogeneous aluminum plate of the same thickness as the lens. The first antisymmetric mode represents the fundamental mode of wave propagation at the design frequency. The refractive indices of the unit cells are calculated using Eq. (4), with phase velocities extracted from the dispersion relations as $c_{GM} = w\,(k_x)/k_x$. Specifically, the phase velocity of the wave propagating through each unit cell is determined by the slope of its dispersion curve. Since w varies nonlinearly with k_x due to the structure's internal resonances, the phase velocity changes with frequency. As a result, the refractive index becomes frequency dependent. Physically, the internal resonances are directly related to the modified effective mass and stiffness resulting from the introduction of blind holes in the structure of the unit cell.

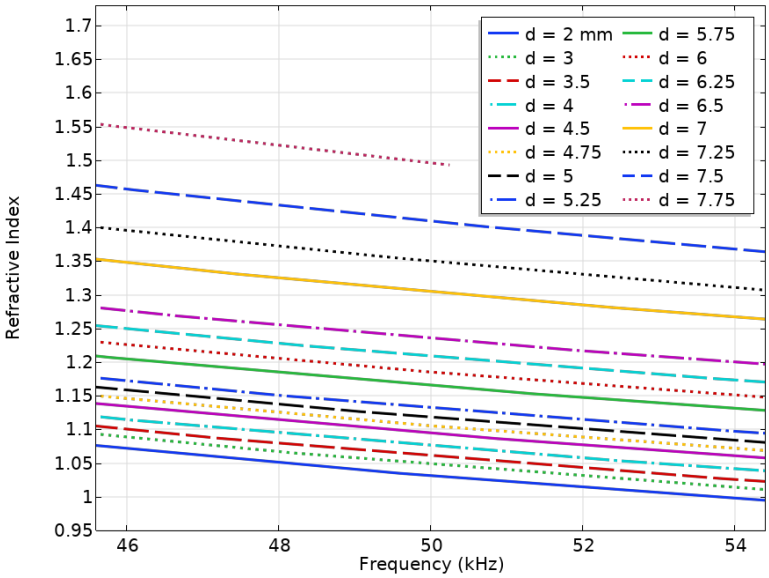

Fig. 2. Refractive index per frequency for unit cells of different diameter blind holes.

By analyzing dispersion curves, phase velocity values are obtained, used to compute the refractive indices, and presented in Figure 4. As illustrated, the refractive indices are strongly frequency dependent. The lowest refractive indices are observed in the unit cell with $d = 2$ *mm*, and as the diameters of blind holes increase, the refractive indices also increase, with the unit cell with $d = 7.75$ *mm* having the highest values. Fig. 2 4 directly results from the dispersion relation analysis. The dispersion diagram of Figure 3 depicts that longitudinal shape modes along the ΓM path exist only up to around 50 *kHz* in the 7.75 mm unit cell; beyond this frequency, other modes may emerge or vanish. This explains why the refractive index line in Figure 4 vanishes past 50 *kHz*—above that point, the longitudinal ΓM modes no longer exist.

Table 1. Refractive index of unit cells of different hole diameters at the design frequency of 50 *kHz*.

Diameter (mm)	Refractive Index
2	1.0314
3	1.0492
4	1.0768
5	1.1185
6	1.1853
6.5	1.2360
7	1.3051
7.5	1.4096
7.75	1.4959
2	1.0314

Table 1 indicates a broad range of refractive indices, from 1.03 to 1.4959, achievable at the design frequency (50 *kHz*) with the proposed unit cells. This wide range is particularly appropriate because it enables the precise design of modified Luneburg lens profiles by carefully arranging unit cells adjacent to one another across multiple concentric layers.

Based on the governing equation of the modified Luneburg lens, three hexagonal lenses are designed for three different focal points (*F=R, 1.5R, 2R*). One of the lenses (*F = R*) is shown in Figure 2. (c). The three aforementioned modified Luneburg lens profiles are discretized to 11 layers, as shown in Fig. **3**. The arrangement of unit cells in concentric layers is determined by each unit cell's refractive index and the required position of that index in the profile.

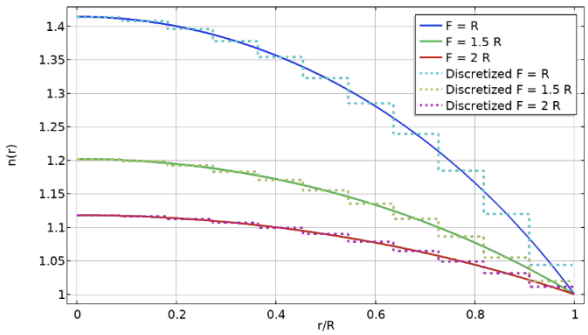

Fig. 3. Discretized Refractive index profile of Luneburg lens.

Table. 2. Blind hole diameters (mm) in each layer for three designed lenses

Layers	$F = R$	$F = 1.5R$	$F = 2R$
1	7.5	6.25	5
2	7.5	6.25	5
3	7.5	6	5
4	7.25	6	4.75
5	7.25	5.75	4.75
6	7	7.5	4.5
7	7	5.25	4
8	6.5	5	3.5
9	6	4	3
10	5	3	2
11	3	2	2

The unit cells with the largest blind holes are located around the center of the lens, and small holes are located toward the edge of the lens. All three lenses have a diameter of 176 *mm* (R = 88 *mm*) and consist of 379 unit cells in 11 layers. Table. 2 includes the corresponding diameters of blind holes in each layer of the three lenses.

The performance of the lens in focusing elastic waves is evaluated using finite element simulations in COMSOL Multiphysics. The solid mechanics module is used to perform a structural analysis in the frequency domain, enabling the derivation of the displacement, velocity, and stress fields. A frequency-domain study (at a design frequency of 50 *kHz*) is used to compute the response of the wave equation in solids to a harmonic wave with respect to particular load distributions. This provides the displacement field (u). The velocity field can then be derived directly by applying the relation $v=i\omega u$, where v is the velocity field, and ω is the angular frequency.

The simulation domain is chosen as a plate with an area of 800×300 mm^2 for $F = R$, 1000×300 mm^2 for $F = 1.5R$, and 1200×300 mm^2 for $F = 2R$, with a thickness of 3 *mm* in all cases. Aluminum with constants of elasticity E = 70 GPa, density = 2700 kg/m3, and Poisson's ratio of $\nu = 0.33$ is considered as the material for this study. A boundary load of $F_z = 1$ N is applied to the left side of the plate, and the other sides are considered as low reflection boundaries. Mesh size is set to be at least 7 mesh elements per wavelength in the design frequency of 50 *kHz*. An image of the meshed geometry of the lens is provided in **Error! Reference source not found.**. (d).

3. Results

The normalized root-mean-square (RMS) velocity fields of Fig. **4** are obtained as a result of simulations. As shown in this figure, elastic wave focusing is obtained by the proposed lenses of this study at three different focal points. In all three cases, the waves are curved toward the focal point of the lens, confirming the lens's gradient-refractive-index profile. It can be observed that

wave concentration is stronger at focal points closer to the lens. Due to inherent aberrations in the focal points of modified Luneburg lenses, as pointed out in section 2, the focal length increases as the focal point moves from *R* to 2*R*. This suggests the possibility of using such a lens to create acoustic/elastic wave jets.

Fig. **5** illustrates the RMS value of velocity over the *y* coordinate. The *xyz* coordinate is placed at the middle of the upper surface of the lens, with *y* being parallel to the width of the domain (y ranges from -150 to 150 *mm* to cover 300 *mm*). As shown in this graph, focusing the elastic wave is achieved by the proposed lens in the vicinity of the intended focal points. The distribution of waves scatters along the *y* axis as the focal point increases, and the lens with *F=R* shows the highest level of focusing of elastic waves based on the maximum velocity reached.

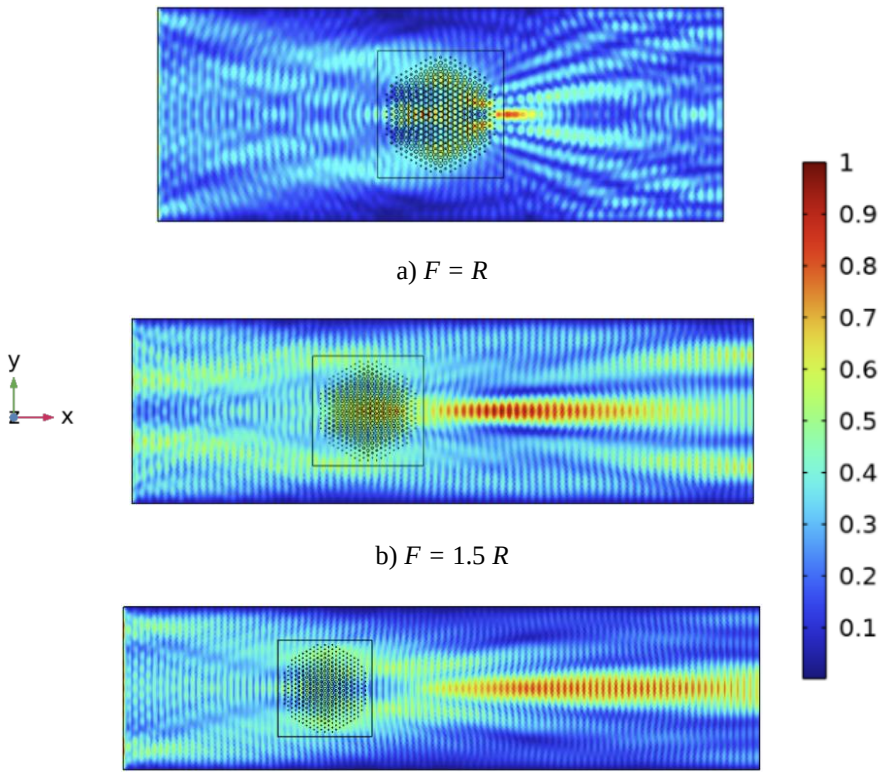

a) $F = R$

b) $F = 1.5\ R$

c) $F = 2\ R$

Fig. 4. Normalized RMS velocity fields in simulation domain 1.

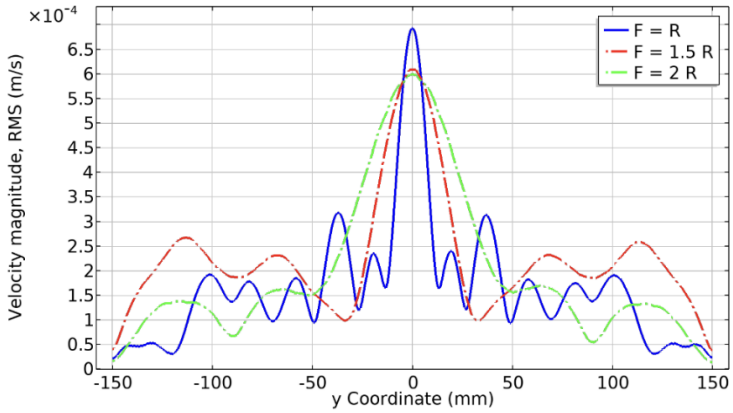

Fig. 5. RMS velocity over the y coordinate.

The three lenses were designed for the working frequency of 50 *kHz*. To further study the performance of these lenses, a frequency study was conducted from 46 *kHz* to 52 *kHz*, and the results are presented in Fig. **6** and **Error! Reference source not found.**. This frequency analysis focuses on three key parameters of focusing: maximum amplification of RMS velocity relative to the reference velocity captured without the lens, full width at half maximum (*FWHM*), and decay length estimated from the point of maximum velocity to ½ of this value. The amplification data indicate that significant focusing behavior occurs over the tested range in all three lenses. For a lens with a focal point of $F=R$, the acceptable amplification (at least 1.5 times the reference velocity) occurs in the range of 49 to 51 *kHz*. The values for 1.5R and 2R lenses are 46-51 kHz and 47-51 *kHz*, respectively. The lens designed to focus at $F=R$ achieves the highest amplification of 5.96 at 50 *kHz*, with subwavelength focusing of $FWHM=0.73\lambda$ and a decay length of 2.14λ. This lens has the narrowest focal zone, with the lowest FWHM of 0.71λ at 51 *kHz*. The other two designed lenses with focal points of $1.5R$ and $2R$ exhibit high amplifications of 4.81 and 4.77 at the design frequency, respectively. Fig. **6** illustrates the normalized RMS velocity fields for the lens designed with a focal point of $F = R$ across the frequency range of 48 kHz to 52 kHz. These images were selected as representative examples because this lens exhibited the highest amplification and sharpest focal zone among the three designs.

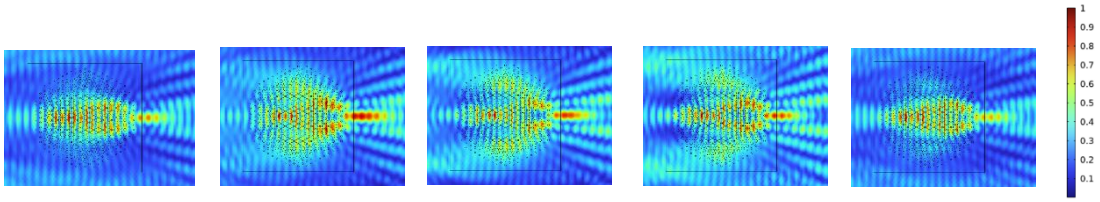

(a) f = 48 kHz (b) f = 49 kHz (c) f = 50 kHz (d) f = 51 kHz (e) f = 52 kHz

Fig. 6. Normalized RMS velocity fields of $F=R$ Lens.

Table 3. Frequency-dependent analysis of the three acoustic metamaterial Luneburg lenses.

Maximum Amplification of RMS Velocity								
Frequency (kHz)		46	47	48	49	50	51	52
Focal Point	F=R	-	-	1.02	3.32	5.96	2.86	1.4
	F=1.5R	2.67	2.27	3.88	4.28	4.81	2.34	1.2
	F=2R	1.3	3.06	4.13	4.51	4.77	1.6	1.29
FWHM								
Frequency (kHz)			49			50		51
Focal Point	F=R		0.78 λ			0.73 λ		0.71 λ
	F=1.5R		1.69 λ			1.64 λ		1.64 λ
	F=2R		3.74 λ			2.54 λ		2.57 λ
Decay Length								
Frequency (kHz)			49			50		51
Focal Point	F=R		2.2 λ			2.14 λ		1.74 λ
	F=1.5R		10.76 λ			10.32 λ		9.87 λ
	F=2R		15.63 λ			15.02 λ		14.42 λ

Although decent amplification is observed in the frequency range under study, the correct functionality of the Luneburg lens, defined as sharp focusing at the pre-designed focal points, is only acceptable between 49 *kHz* and 51 *kHz*. In this narrower band, all three lenses focus waves at their pre-intended focal points. For instance, as the frequency changes to 46 *kHz*, the lens intended for $F=1.5R$ still has a high amplification of 2.67 at that position, but the peak amplification no longer occurs at the expected location; instead, it occurs closer to the lens. This deviation of the focal point is due to the dispersive behavior of the metamaterial's unit cells. As shown in Fig. **2**, unit cells' refractive indices are frequency-dependent. As a result, the refractive index profiles no longer match the intended focal point's Luneburg profile. For example, a unit cell with a blind hole diameter of 3 *mm* that exhibits an index of 1.05 at 50 *kHz*, shifts this value to 1.09 at 46 *kHz*, resulting in a reconfigured refractive index profile of the lens. The waves will no longer concentrate at the intended focal point but instead focus at a new and unwanted focal point. While this still results in significant focusing and amplification, the lens no longer functions as intended by the designer. On the other hand, if achieving a long focal length is desirable in applications of the lenses instead of the exact position of the focal point, the lenses can be assumed to operate over an even broader frequency range. These lenses can achieve decay lengths of up to $15.63l$ in the case of $F=2R$, which is excellent for vibration-based energy harvesting techniques and acoustic jet applications. Therefore, while the designed lenses exhibit excellent broadband behavior and can still produce high amplification over a wider frequency range, their intended functionality is constrained to a narrower 2 *kHz* band around the design frequency of 50 *kHz*.

Comparing the results of this study with previous work is difficult because the reported metamaterial lenses for elastic waves have different objectives. However, several studies remain useful references for this purpose. Table 3 provides a comparison of available key performance parameters, including operating frequency, full width at half maximum (*FWHM*), amplification, and lens design method. Previous studies focused primarily on lens design methods with a fixed focal point. They did not investigate methods for passively positioning the focus at different locations, such as the one presented in this study. In contrast, the design approach presented in this study enables arbitrary placement of the focal point through structural modification. The lens designed for *F=R* achieved the highest amplification among the compared works, along with subwavelength focusing. The results presented here show higher amplification values even for *F=1.5R* and *2R* lenses. Although the *FWHM* values for these lenses are not as sharply focused or as subwavelength as those of others, they still represent localized wave concentrations at their focal points. This highlights the effectiveness of the proposed design method.

Table 3. Comparison of the reported results from acoustic metamaterial lenses for elastic waves focusing.

Reference	Frequency (kHz)	FWHM	Amplification	
Yang et al. [16]	16-19 (Results for 16 kHz)	-	3	Graded negative refractive index plate lens.
Quadrelli et al. [17]	0.321	0.59λ	-	Double-negative piezoelectric metamaterial.
Zhao et al. [18]	50, 100, 150, 200 (Results for 100 kHz)	0.5λ	4	Structural Generalized Luneburg lens (GLL), localization of energy between 2 focal spots.
Tol et al. [19]	50	-	3.7	Gradient-Index Phononic Crystal Lens (GRIN-PCL) with hyperbolic secant gradient refractive index profile.
Current study for the lens with *F=R*	49-51 (Results for 50 kHz)	0.73λ	5.96	Adjustable focal point design method with gradient-index acoustic metamaterial based on modified Luneburg refractive index profile.
Current study for the lens with *F=1.5R*	49-51 (Results for 50 kHz)	1.64λ	4.81	
Current study for the lens with *F=2R*	49-51 (Results for 50 kHz)	2.54λ	4.77	

Conclusion

This paper demonstrated a novel design method for acoustic lenses with predetermined focal points of elastic waves based on the modified Luneburg refractive index profile. This was achieved by designing and simulating three lenses for focusing elastic waves at three focal points. The hexagonal unit cells presented in this study have design parameters that enable them to achieve a

wide range of refractive indices, ranging from 1.0314 to 1.4959 at the design frequency of 50 *kHz*. Dispersion curves are calculated via finite-element method simulations, and as a result, the refractive index is derived for each unit cell at the design frequency. The lenses are formed by arranging hexagonal unit cells with blind holes of varying diameters based on modified Luneburg lens refractive index profiles. The results from numerical wave simulations confirmed accurate focusing of waves at the intended focal points at $F = R$, $1.5R$, and $2R$, validating the effectiveness of the design. The lens designed for $F = R$ achieved the highest level of focusing based on maximum velocity, with the highest amplification of 5.96 times the reference velocity. As the focal point shifted from R to $2R$, the wave distribution became scattered along the focal axis. Furthermore, a frequency-dependent study from 46 *kHz* to 52 *kHz* revealed that precise Luneburg lens focusing is achieved within the 49–51 *kHz* band. Outside this band, significant amplification is observed, while focal points shift due to changes in the refractive index profile. The $F = R$ lens produces a subwavelength focal zone, achieving a minimum *FWHM* of 0.71λ at 51 *kHz*, whereas the $F = 1.5R$ and $F = 2R$ designs yield focal widths of 1.6λ and 2.6λ. High decay-length values are achieved with these lenses. For instance, a decay length of up to 15.63λ with the $F = 2R$ lens emphasizes its potential for applications requiring a long focal region. The adaptability and structural integrity of the proposed design make this approach a promising path for advanced wave manipulation. The results of this study offer significant potential for applications in areas such as industrial non-destructive testing, imaging, and energy harvesting.

References

[1] J. Zhang, B. Hu, S. Wang, Review and perspective on acoustic metamaterials: From fundamentals to applications, Applied Physics Letters, Vol. 123, Iss.1,(2023)

[2] G. Liao, C. Luan, Z. Wang, J. Liu, X. Yao, J. Fu, Acoustic metamaterials: A review of theories, structures, fabrication approaches, and applications, Advanced Materials Technologies, Vol. 6, Iss.5,(2021)

[3] M. Zarastvand, M. Ghassabi, R. Talebitooti, Acoustic Insulation Characteristics of Shell Structures: A Review, Archives of Computational Methods in Engineering, Vol. 28, Iss.2,(2021)

[4] M. Zarastvand, M. Ghassabi, R. Talebitooti, A Review Approach for Sound Propagation Prediction of Plate Constructions, Archives of Computational Methods in Engineering, Vol. 28, Iss.4,(2021)

[5] M. Zarastvand, M. Ghassabi, R. Talebitooti, Prediction of acoustic wave transmission features of the multilayered plate constructions: A review, Journal of Sandwich Structures & Materials, Vol. 24, Iss.1,(2022)

[6] P. Sun, S. Xu, X. Wang, L. Gu, X. Luo, C. Zhao, Z. Huang, Sound absorption of space-coiled metamaterials with soft walls, International Journal of Mechanical Sciences, Vol. 261,(2024)

[7] M. Sun, X. Fang, D. Mao, X. Wang, Y. Li, Broadband acoustic ventilation barriers, Physical Review Applied, Vol. 13, Iss.4,(2020)

[8] N. Jiménez, V. Romero-García, L.M. García-Raffi, F. Camarena, K. Staliunas, Sharp acoustic vortex focusing by Fresnel-spiral zone plates, Applied Physics Letters, Vol. 112, Iss.20,(2018)

[9] Y. Zhu, B. Assouar, Multifunctional acoustic metasurface based on an array of Helmholtz resonators, Physical review B, Vol. 99, Iss.17,(2019)

[10] L. Zhao, T. Horiuchi, M. Yu, Broadband acoustic collimation and focusing using reduced aberration acoustic Luneburg lens, Journal of Applied Physics, Vol. 130, Iss.21,(2021)

[11] Y. Jin, X. Fang, Y. Li, D. Torrent, Engineered diffraction gratings for acoustic cloaking, Physical Review Applied, Vol. 11, Iss.1,(2019)

[12] D. Ozevin, S. Tol, "Role of acoustic metamaterials and phononic crystals in sensing and damage detection in solids," in *The Rise of Smart Cities*: Elsevier, 2022, pp. 115-137.

[13] H. Selim, R. Picó, J. Trull, M.D. Prieto, C. Cojocaru, Directional ultrasound source for solid materials inspection: Diffraction management in a metallic phononic crystal, Sensors, Vol. 20, Iss.21,(2020)

[14] Z. Wen, W. Wang, A. Khelif, B. Djafari-Rouhani, Y. Jin, A perspective on elastic metastructures for energy harvesting, Applied Physics Letters, Vol. 120, Iss.2,(2022)

[15] L. Zhao, C. Bi, M. Yu, Acoustic Lenses Design based on the Rays Inserting Method, arXiv preprint arXiv:2208.06951, Vol.,(2022)

[16] F. Yang, Z. Tan, X. Han, C. Cho, A graded negative refraction-index phononic crystals plate lens for focusing A0 mode Lamb wave and energy harvesting, Results in Physics, Vol. 31,(2021)

[17] D. Enrico Quadrelli, J. Marconi, F. Braghin, A. Erturk, Subwavelength negative refraction and flexural wave lens design via resonant double-negative piezoelectric metamaterial, Smart Materials and Structures, Vol. 33, Iss.2,(2024)

[18] L. Zhao, H. Kim, M. Yu, Structural Luneburg lens for broadband ultralong subwavelength focusing, Mechanical Systems and Signal Processing, Vol. 182,(2023)

[19] S. Tol, F.L. Degertekin, A. Erturk, Gradient-index phononic crystal lens-based enhancement of elastic wave energy harvesting, Applied Physics Letters, Vol. 109, Iss.6,(2016)

[20] S. Tol, F.L. Degertekin, A. Erturk, Phononic crystal Luneburg lens for omnidirectional elastic wave focusing and energy harvesting, Applied Physics Letters, Vol. 111, Iss.1,(2017)

[21] L. Zhao, C. Bi, H. Huang, Q. Liu, Z. Tian, A review of acoustic Luneburg lens: Physics and applications, Mechanical Systems and Signal Processing, Vol. 199,(2023)

[22] W.S. Gan, New acoustics, based on metamaterial, in *Proceedings of Meetings on Acoustics*, 2012, Vol. 15, Iss. 1: Acoustical Society of America, p. 030003.

[23] V. Romero-Garcia, A.-C. Hladky-Hennion, Fundamentals and applications of acoustic metamaterials: from seismic to radio frequency, John Wiley & Sons, 2019.